Estimating in situ rock mass strength and elastic modulus of granite from the Soultz-sous-Forêts geothermal reservoir (France)

Marlène Villeneuve, Michael Heap, Alexandra Kushnir, Tao Qin, Patrick Baud, Guanglei Zhou, Tao Xu

Villeneuve *et al. Geotherm Energy (2018) 6:11*
https://doi.org/10.1186/s40517-018-0096-1

Geothermal Energy

RESEARCH Open Access

Estimating in situ rock mass strength and elastic modulus of granite from the Soultz-sous-Forêts geothermal reservoir (France)

Marlène C. Villeneuve[1*], Michael J. Heap[2], Alexandra R. L. Kushnir[2], Tao Qin[3], Patrick Baud[2], Guanglei Zhou[4] and Tao Xu[4]

*Correspondence: marlene.villeneuve@canterbury.ac.nz
[1] Department of Geological Sciences, University of Canterbury, Private Bag 4800, Christchurch 8140, New Zealand
Full list of author information is available at the end of the article

Abstract

Knowledge of the strength and elastic modulus of a reservoir rock is important for the optimisation of a particular geothermal resource. The reservoir rock for many geothermal projects in the Upper Rhine Graben, such as those at Soultz-sous-Forêts and Rittershoffen (both France), is porphyritic granite. High fracture densities (up to ~ 30 fractures/m) in this reservoir rock require that we consider the strength and elastic modulus of the rock mass, rather than the intact rock. Here we use uniaxial and triaxial deformation experiments performed on intact rock coupled with Geological Strength Index assessments—using the wealth of information from core and borehole analyses—to provide rock mass strength and elastic modulus estimates for the granite reservoir at Soultz-sous-Forêts (from a depth of 1400 to 2200 m) using the generalised Hoek–Brown failure criterion. The average uniaxial compressive strength and elastic modulus of the intact granite are 140 MPa (this study) and 40 GPa (data from this study and the literature), respectively. The modelled strength of the intact granite is 360 MPa at a depth of 1400 m and increases to 455 MPa at 2200 m (using our estimate for the empirical m_i term of 30, determined using triaxial and tensile strength measurements on the intact granite). Strength of the rock mass varies in accordance with the fracture density and the extent and nature of the fracture infill, reaching lows of ~ 40–50 MPa (in, for example, the densely fractured zones in EPS-1 at depths of ~ 1650 and ~ 2160 m, respectively) and highs of above 400 MPa (in, for example, the largely unfractured zone at a depth of ~ 1940–2040 m). Variations in rock mass elastic modulus are qualitatively similar (values vary from 1 to 2 GPa up to the elastic modulus of the intact rock, 40 GPa). Our study highlights that macrofractures and joints reduce rock mass strength and should be considered when assessing the rock mass for well stability and rock mass deformation due to stress redistribution in the reservoir. We present a case study to demonstrate how a simple and cost-effective engineering method can be used to provide an indication of the in situ strength and elastic modulus of reservoir rock masses, important for a wide range of modelling and stimulation strategies. We recommend that the effect of macrofractures on rock mass strength and stiffness be validated for incorporation into geomechanical characterisation for geothermal reservoirs worldwide.

Keywords: Borehole, Well, Fractures, Failure criteria

Background

Geothermal projects in the Upper Rhine Graben (URG)—a Cenozoic rift valley that runs along the border between France and Germany—aim to harness thermal gradient anomalies (100 °C/km) attributed to hydrothermal circulation within the fractured Palaeozoic granitic basement and the overlying Permian and Triassic sediments (Pribnow and Schellschmidt 2000; Guillou-Frottier et al. 2013; Magnenet et al. 2014).

The granite reservoir rock (from the sites at Soultz-sous-Forêts and Rittershoffen, both France; Fig. 1) has been the subject of numerous studies since the inception of the Soultz-sous-Forêts enhanced geothermal system (EGS) project about 30 years ago (Kappelmeyer et al. 1991; Baria et al. 1999; Gérard et al. 2006). It has been characterised, for example, in terms of its fracture density, structure, alteration, thermal conductivity, and permeability (e.g. Rummel 1992; Ledésert et al. 1993, 1999, 2010; Genter and Traineau 1996; Dezayes et al. 2000, 2010; Surma and Géraud 2003; Sausse et al. 2006, 2010; Bartier et al. 2008; Géraud et al. 2010; Vidal et al. 2017; Meller and Ledésert 2017). However, there are few published data on the mechanical behaviour, strength and stiffness (elastic modulus) of the URG reservoir granite rock mass.

There is a rich literature on the mechanical behaviour of intact, typically fresh, granite. Uniaxial and triaxial experiments have explored dilatancy and brittle behaviour (e.g. Brace et al. 1966; Byerlee 1967; Tapponnier and Brace 1976; Wong 1982a; Lockner 1998; Eberhardt et al. 1999; Oda et al. 2002), and high-temperature uniaxial and triaxial experiments have studied the influence of temperature on brittle failure (e.g. Wong 1982b; Xu et al. 2008; Shao et al. 2015; Kumari et al. 2017) and "transitional" and ductile behaviour (e.g. Tullis and Yund 1977; Violay et al. 2017). The elastic properties of granite have been similarly well studied (e.g. Sano et al. 1992; Heap and Faulkner 2008; Blake et al. 2013; Blake and Faulkner 2016).

However, the results of the aforementioned studies cannot be directly applied to the URG granites, for two principal reasons. First, the granites of the URG contain very large K-feldspar crystals (long axes up to several tens of mm in length; Fig. 2). Second, the URG granites can be intensely hydrothermally altered (Ledésert et al. 1999; Bartier et al. 2008; Ledésert et al. 2010). Research in volcanic and geothermal systems has shown that alteration can have a large impact on intact rock strength (e.g. Pola et al. 2012, 2014; Frolova et al. 2014; Heap et al. 2015; Siratovich et al. 2016; Wyering et al. 2014, 2015). Granites typically used in rock deformation experiments are selected for their small and homogenous crystal sizes (< 1 mm) and their pristine (fresh, unaltered) nature.

Further, and pertinent to this study and many geothermal reservoirs, the high fracture densities within the URG granites—reaching up to ~ 30 fractures/m (Genter and Traineau 1996)—question the direct applicability of deformation experiments performed in nominally intact rock (as discussed in Richards and Read 2007). In these intensely fractured zones, the contribution of the fractures to the rock mass strength and stiffness must be considered in geotechnical practices.

We provide here estimates of the in situ rock mass strength (using the generalised Hoek–Brown criterion commonly used in engineering; Hoek et al. 2002) and rock mass elastic modulus (using the Hoek–Diederichs equation; Hoek and Diederichs 2006) for

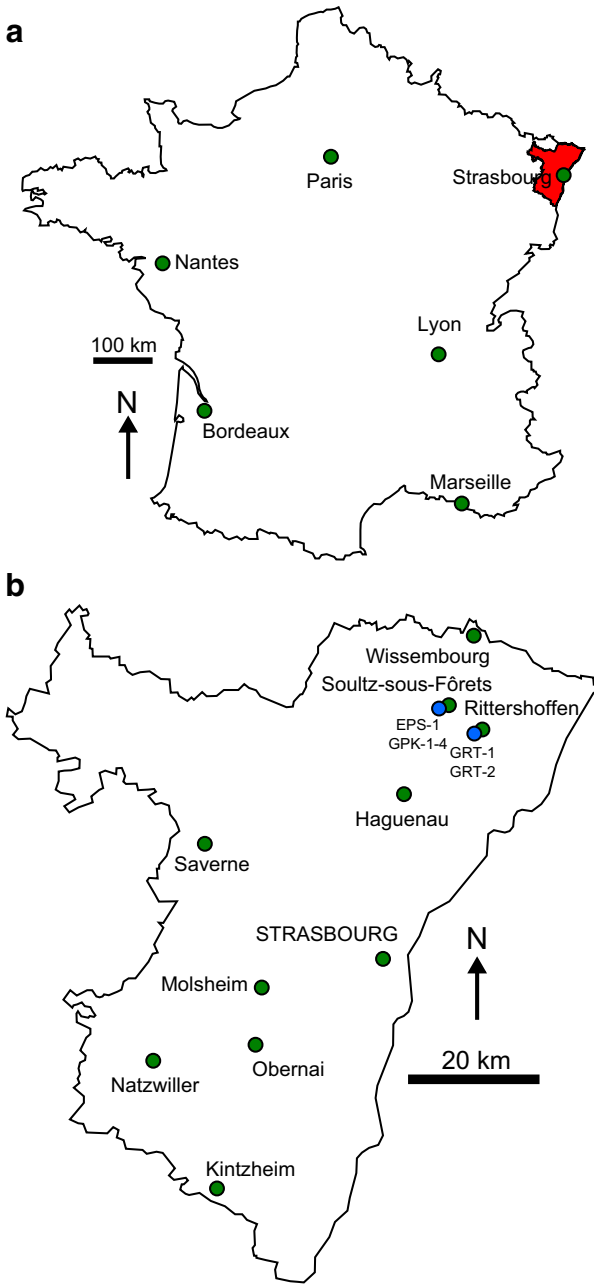

Fig. 1 **a** Map of France showing the location of the Bas-Rhin (Lower Rhine) department of Alsace (in red). **b** Map of the Bas-Rhin department of Alsace (shown in red in **a**) showing the location of the major cities/towns and the geothermal sites and geothermal boreholes of Soultz-sous-Forêts and Rittershoffen (Figure modified from Heap et al. (2017))

the granite reservoir at Soultz-sous-Forêts. These values are crucial input parameters for reservoir-scale modelling (e.g. Bérard and Cornet 2003; Yoon et al. 2014; McClure and Horne 2013 and references therein) and guiding stimulation design (e.g., Cipolla et al. 2008; Meller and Ledésert 2017).

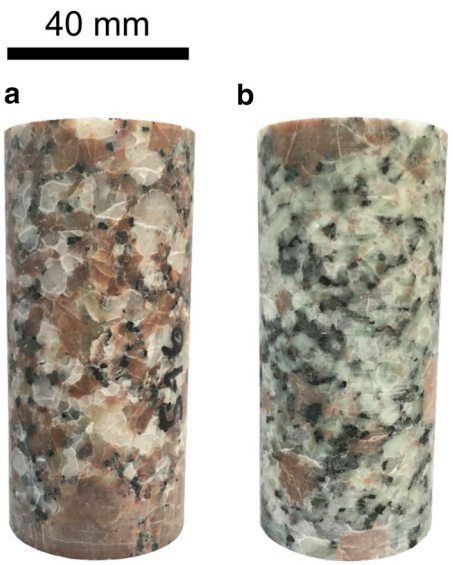

Fig. 2 Photographs of representative samples taken from EPS-1 (Soultz-sous-Forêts) geothermal borehole. All samples were re-cored to a diameter of 40 mm. All samples are from the uppermost (facies 1; see text for details) standard porphyritic granite. **a** An example of a sample of standard porphyritic granite from the palaeo-weathered zone. **b** An example of a sample of standard porphyritic granite (from below the palaeo-weathered zone)

We selected the widely used generalised Hoek–Brown failure criterion (Hoek et al. 2002) to estimate the strength of the rock mass as a function of depth. The generalised Hoek–Brown failure criterion is the suggested method of the international society of rock mechanics (ISRM) to characterise rock mass strength (Eberhardt 2012). This failure criterion combines intact rock strength and rock mass characterisation values to provide strength values for an equivalent isotropic fractured rock mass. For over 30 years it has been the geotechnical industry state of practice for deriving rock mass strength parameters for slope stability analysis (e.g. Brideau et al. 2011; Shen et al. 2012; Schaefer et al. 2013; Dotta et al. 2017), tunnel design (e.g. Martin et al. 1999; Cai et al. 2004; Genis et al. 2007; Zhang et al. 2011), mining geotechnics (e.g. Alber et al. 2009) and more recently in reservoir geomechanics (e.g. Diesman et al. 2013).

We selected the Hoek–Diederichs (2006) equation to derive rock mass elastic stiffness parameters because it uses a parallel methodology for combining intact and rock mass characteristics to estimate stiffness for an equivalent isotropic rock mass. Both methods follow a similar approach: (1) obtain intact rock strength and stiffness properties, using laboratory values or field estimates; (2) obtain rock mass characterisation using field mapping or borehole studies; and (3) combine the two datasets using the Hoek–Brown (strength) or Hoek–Diederichs (stiffness) equations.

This paper will follow this procedure for the URG granite, starting with intact rock strength and stiffness measurements from this study, combined with values of strength and stiffness from published and unpublished reports. This is followed by a rock mass characterisation using published borehole studies. Finally, the intact rock and rock mass characteristics are combined to derive rock mass strength and stiffness estimates at the wellbore scale (from a borehole depth of ~1400 to ~2200 m in EPS-1) using these

commonly obtained site investigation data. The objective is to highlight the effect of macrofractures on rock mass strength and stiffness, even at the wellbore scale, and to demonstrate that modelling the rock mass using only intact rock strength and stiffness parameters can overestimate these values.

Methods

Upper Rhine Graben granites

The granitic basement in the URG, the principal heat-exchanger for projects such as those at Soultz-sous-Forêts and Rittershoffen, chiefly comprises a porphyritic granite containing quartz, plagioclase, K-feldspar megacrysts, biotite, hornblende, accessory apatite, titanite and magnetite (Traineau et al. 1991; Genter and Traineau 1992; Hooijkaas et al. 2006).

In detail, the Palaeozoic granitic basement of the URG comprises four facies (Traineau et al. 1991; Hooijkaas et al. 2006). (1) Standard porphyritic granite (a monzogranite) (measured depth ~1400 to ~2800 m at Soultz-sous-Forêts). The top ~150 m of this facies is coloured red as a result of palaeo-weathering: the primary iron-bearing minerals (biotite, magnetite and amphibole) are partly altered into iron-hydroxide or hematite (Fig. 2 shows photographs of samples taken from the EPS-1 core within this top porphyritic facies). (2) Standard porphyritic granite with intense vein alteration (depth ~2800 to ~3500 m). (3) Biotite- and amphibole-rich granite that gradually evolves into the standard porphyritic granite with depth (depth ~3500 to ~4800 m). (4) "Two-mica" granite (~4800 to ~5100 m). The reservoir granite is overlain by a ~1400 m-thick (at Soultz-sous-Forêts) Mesozoic to Cenozoic sedimentary succession (although there is a thin (~9 m) layer of Permian sandstone at the granite-sediment interface) (Vidal et al. 2015; Aichholzer et al. 2016; Griffiths et al. 2016; Heap et al. 2017; Kushnir et al. 2018).

The compressive strength of granite (depth = 1377–2002 m) taken from GPK-1 (see Fig. 1 for location) was found to range between 120 and 485 MPa at a confining pressure of 40 MPa (Rummel 1992), and uniaxial compressive strength (UCS) values between 100 and 130 MPa are reported for unaltered granite from Soultz-sous-Forêts in an unpublished report (Valley and Evans 2006). Average values of dynamic (estimated from P- and S-wave velocities and measurements of bulk density) and static (from three-point bending tests) elastic modulus for granite sourced from GPK-1 were found to be 69 and 38 GPa, respectively (Rummel 1992). Unpublished data on granite taken from EPS-1 and GPK-1 show that static elastic modulus can range from ~50 to ~75 GPa (Rummel et al. 1989; Schäfer 1990; Valley and Evans 2006) and that the dynamic elastic modulus can range from ~60 to ~70 GPa on nominally dry samples (Schäfer 1990; Rummel and König 1991; Rummel et al. 1992; Rummel and Schreiber 1993) and up to ~90 GPa for saturated cores (Schäfer 1990).

Case study: granite from Soultz-sous-Forêts (EPS-1)

The materials used for this study were taken from exploration borehole EPS-1 from the Soultz-sous-Forêts geothermal site (Fig. 1). Granite cores were sampled from three depths within the standard porphyritic granite (monzogranite) facies: 1420, 1558 and 1915 m. The sample collected from 1420 m depth is very close to the contact between the granite and sedimentary cover (at a depth of ~1400 m) and is therefore within the

palaeo-weathered zone. The studied granites have essentially identical crystal sizes and distributions (Fig. 2) and almost identical mineral compositions. The primary iron-bearing minerals (biotite, magnetite and amphibole) are partly altered into iron-hydroxide or hematite in the palaeo-weathered horizon (Fig. 2a), but are fresh in the deeper zones (Fig. 2b). Sampling these two visibly different horizons was important to understand whether we should treat the granite from ~1400 to ~2200 m (the depth range for the structural data for the borehole) as one or two mechanically distinct layers.

Seventeen cylindrical samples (40 mm in diameter) were prepared from the cores collected (two from the 1420 m sample, 12 from the 1558 m sample, and three from the 1915 m sample) and precision-ground to a nominal length of 80–85 mm. These samples were cored so that their axes were parallel to the plunge of the EPS-1 borehole. Photographs of representative examples (from the weathered and non-weathered horizons) of the cylindrical samples are provided in Fig. 2. The 12 samples from a depth of 1558 m were split into two categories: six that contained large phenocrysts and six that did not.

Intact rock failure criterion

The Hoek–Brown failure criterion for intact rock provides a non-linear fit to triaxial data according to:

$$\sigma_1' = \sigma_3' + C_o\left(m_i\frac{\sigma_3'}{C_o} + 1\right)^{0.5} \tag{1}$$

where σ_1' and σ_3' are the effective maximum and minimum principal stresses, respectively, in MPa; C_o is the uniaxial compressive strength, in MPa, and m_i is a unitless empirical fitting parameter related to the lithology (Eberhardt 2012). The two unknowns in Eq. 1 are C_o and m_i.

C_o was determined using laboratory experiments. All of the 40 mm-diameter cylindrical samples were first dried (in an oven at 60 °C for at least 48 h). Samples from each depth (two samples from a depth of 1420 m, two samples containing large phenocrysts from 1558 m, two samples without large phenocrysts from 1558 m, and three samples from 1915 m) were deformed in a uniaxial press at a constant strain rate of 10^{-5} s^{-1} until macroscopic failure. The peak stress recorded at macroscopic failure is the uniaxial compressive strength, C_o. Prior to destructive testing the connected porosity of each 40 mm-diameter sample was determined using the saturation-buoyancy technique (Ulusay and Hudson 2007).

In geotechnical engineering, there are two accepted methods for obtaining m_i: (1) through triaxial testing and curve fitting of the test data (as in Hoek and Brown 1980) or (2) using the m_i estimates table found in the database in the commercially available software RocData (Rocscience 2017). The m_i value for granite in the RocData table is 32 ± 3 (Rocscience 2017). Although this value is based on test data on granite, we wanted to explore the impact of different m_i values on granite as a function of weathering or hydrothermal alteration (since we know that the URG granites can be intensely hydrothermally altered; Ledésert et al. 1999, 2010; Bartier et al. 2008). We conducted eight triaxial deformation experiments using a "Hoek Cell" hydrostatic pressure vessel. These

experiments were only performed on samples from a depth of 1558 m. Four experiments were performed at confining pressures of 5, 10, 20 and 30 MPa on samples that contained large phenocrysts, and four experiments were performed (at the same confining pressures) on samples without large phenocrysts. These experiments were all performed at a constant strain rate of 10^{-5} s^{-1} until macroscopic failure. The results of these uniaxial and triaxial tests were then used to derive a representative range of m_i values by curve fitting using the laboratory data fitting function in RocData (Rocscience 2017). We used the modified cuckoo fit algorithm, basic error summation and absolute error type.

The Hoek–Brown failure criterion solved using the algorithm in RocData will tend to over- or underestimate the tensile strength (Sari 2012). To provide a tensile strength cut-off we conducted eight indirect tensile strength tests on 40 mm wide, 20–24 mm thick discs from the sample at 1558 m depth in accordance with the ISRM standard (Ulusay and Hudson 2007; Li and Wong 2013). Again, we noted whether the samples had visibly large phenocrysts. We loaded the samples diametrically in compression at a stress rate of 0.06 MPa/s until tensile rupture, indicated by the development of a throughgoing fracture. The indirect tensile strength, σ_t, was determined as follows:

$$\sigma_t = \frac{2P}{\pi 2Rt} \tag{2}$$

where P is the applied load at tensile rupture, R is the sample radius and t is the thickness of the disc.

Intact rock elastic modulus

The elastic modulus describes the linear elastic deformation response of rock under deformation. The static elastic modulus of an intact rock, E_i, is typically calculated as the slope of the stress–strain curve of a rock deforming under uniaxial compression (Ulusay and Hudson 2007). We calculated the static elastic modulus for our samples from the UCS and the triaxial tests. Static elastic modulus was only determined for the samples from a depth of 1558 m; the modulus could not be determined for the other five UCS tests (on samples from depths of 1420 and 1915 m) due to technical problems. In addition, values for static elastic modulus have been found to range from ~ 50 to 75 GPa for granites from the URG (Rummel et al. 1989; Schäfer 1990; Rummel and König 1991; Rummel et al. 1992; Rummel 1992; Rummel and Schreiber 1993; Valley and Evans 2006). These data, largely from unpublished reports, are summarised in Table 1.

Rock mass failure criterion

With our values for C_o and m_i, we used the generalised form of the Hoek–Brown failure criterion for fractured rock masses (as in Hoek et al. 2002), using published data about the structure and nature of the fractures in the rock mass. The generalised Hoek–Brown failure criterion is similar to Eq. 1, but with additional empirical fitting parameters to account for the lower strength of fractured rock masses (Hoek et al. 2002):

$$\sigma_1' = \sigma_3' + C_o\left(m_b\frac{\sigma_3'}{C_o} + s\right)^a \tag{3}$$

where m_b, s and a are unitless fitting parameters, calculated as follows (Hoek et al. 2002):

Table 1 Summary of the elastic moduli reported for URG granites from EPS-1 and GPK-1. From (Rummel et al. 1989; Schäfer 1990; Rummel and König 1991; Rummel et al. 1992; Rummel 1992; Rummel and Schreiber 1993; Valley and Evans 2006)

Type	Average intact elastic modulus	Method	References
Static	49 ± 4	Triaxial compression (40 MPa confinement)	Schäfer (1990)
Static	73 ± 6	Three-point bending tests (62 mm cores)	Rummel et al. (1989)
Static	70 ± 6	Three-point bending tests (30 mm cores)	Rummel et al. (1989)
Static	38 ± 8.5	Three-point bending tests	Rummel (1992)
Static	51 ± 6.6	Uniaxial compression tests	Valley and Evans (2006)
Dynamic	62 ± 5 (dry)	Elastic wave velocities	Schäfer (1990)
	88 ± 4 (wet)		
Dynamic	64 ± 8	Elastic wave velocities	Rummel and König (1991)
Dynamic	71 ± 5	Elastic wave velocities	Rummel et al. (1992)
Dynamic	69	Elastic wave velocities	Rummel (1992)
Dynamic	59 ± 6 (axial)	Elastic wave velocities	Rummel and Schreiber (1993)
	65 ± 10 (radial)		

$$m_{\mathrm{b}} = m_i e^{\left(\frac{\mathrm{GSI}-100}{28-14D}\right)} \tag{4}$$

$$s = e^{\left(\frac{\mathrm{GSI}-100}{9-3D}\right)} \tag{5}$$

$$a = \frac{1}{2} + \frac{1}{6}\left(e^{-\frac{\mathrm{GSI}}{15}} + e^{\frac{-20}{3}}\right) \tag{6}$$

where D is a unitless disturbance factor related to blasting damage in large excavations (Hoek et al. 2002). Well drilling does not use explosives that would induce damage and open the fractures, thus $D = 0$ (we provide the full equation here for completeness). In addition, $D = 0$ for an undisturbed rock mass at high confining pressure, such as the rock mass of a geothermal reservoir.

GSI is the geological strength index (Marinos et al. 2005), a unitless value obtained using an observational method to assess rock mass characteristics with a chart (Fig. 3). Simply put, the GSI combines the rock mass structure (for example fracture density) and fracture quality (for example, weathering or infilling) to derive a value that can be used in Eqs. 4–6, along with D, to create a rock mass failure criterion using Eq. 3. Rock mass structure is typically assessed by comparing the schematics along the vertical axis of Fig. 3 to visual observations of the rock mass, such that the characterisation of the rock mass blockiness is based on the scale of the problem. Blockiness requires intersecting joint sets that define interlocked blocks, rather than a single joint set that defines a structural anisotropy. The key characteristics to assess surface quality are roughness, weathering and infill related to mechanical and chemical deterioration of the fracture surfaces. These can be easily observed from core, but in the absence of core, wireline data (such as resistivity, Muramoto and Elders 1984), could be used to link alteration to fracture

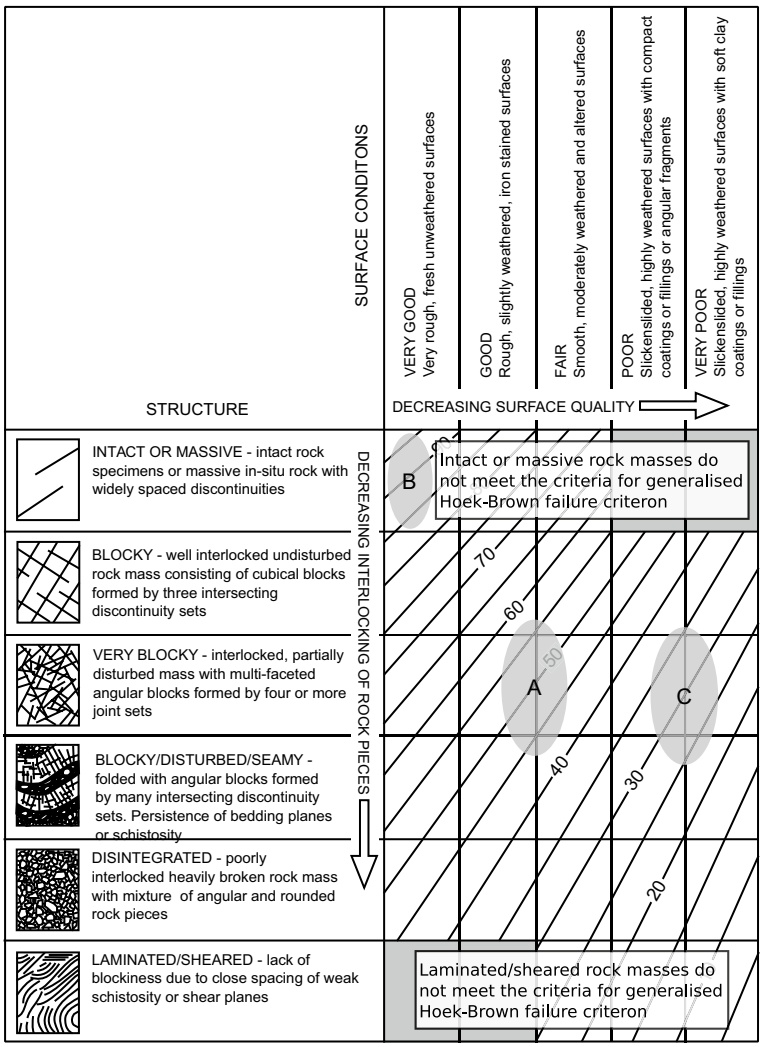

Fig. 3 Chart for obtaining geological strength index (GSI). The positions of the three 25 m-interval rock masses from Fig. 6 are shown on the chart. Note that the highest and lowest category should not be used for the generalised Hoek–Brown failure criterion (Modified from Marinos et al. (2005))

surface quality. The intersection of these two categories results in the GSI estimate, typically presented as a five to ten point range.

For core studies it is not possible to use the chart directly. Hoek et al. (2013) proposed a method for quantifying GSI using rock quality designation (RQD; as defined by Deere 1963) for the structure axis, and the Joint Condition rating $JCond_{89}$ (incorporating persistence, aperture, roughness, infilling and weathering, as defined by Bieniawski 1989) for the surface condition axis. This provides a clear methodology for deriving GSI using a formula, which removes some subjectivity and observer error or variability, although RQD and $JCond_{89}$ are still based on observation rather than measurement. More recent discussions of subjectiveness of rock mass descriptions (e.g. Bertuzzi et al. 2016; Pells et al. 2017) have highlighted that even well-established procedures, such as RQD, result in variable assessments of the rock mass. Because the

EPS-1 core was not assessed for RQD and due to the limitations of RQD noted in the literature, we have used a geometric, scale-dependent assessment of rock mass structure based on fracture frequency. Similarly, due to lack of information about waviness, roughness and persistence of the fractures, we cannot use $JCond_{89}$ or J_C directly. However, Cai et al. (2004) state that joint alteration has the most impact on the joint condition factor and can reduce it by more than one order of magnitude. This, coupled with the statement from Genter and Traineau (1996) that 95.5% of joints are naturally sealed, suggests that the infilling will dominate the joint condition rather than the joint roughness or waviness and thus we have used the infilling to determine joint condition.

Clearly, the degree of interlocking of the blocks cannot be directly assessed from drill core, unless joint orientations are recorded and used to define joint sets, which are then used to determine blockiness (for example using the method presented in Cai et al. 2004). Since this is not always possible for historic data and, for many current borehole logs or core, the GSI derived for analysis must be used in consideration of the inherent uncertainty regarding the degree of interlocking arising from the borehole or drill core study. In field studies, Bertuzzi et al. (2016) found that the quantification method proposed by Hoek et al. (2013) provides similar results to using the look-up chart method despite RQD not providing any explicit information about interlocking.

This leads us to a discussion of scaling considerations. As the scale relationship, or ratio, between the problem being analysed (i.e. wellbore, cavern, slope, reservoir) and the scale of the blocks making up the rock mass increases, the rock mass failure mechanism changes from the failure of intact rock, to the failure along discreet fracture planes to, finally, failure of the rock mass. Hoek and Brown (1980) state that the Hoek–Brown failure criterion is for intact rocks and rock masses that behave as an equivalent isotropic medium. This occurs under two scale relationship conditions (Fig. 4):

1. The problem being analysed is surrounded by intact rock (use Eq. 1).
2. The problem being analysed is surrounded by many joint sets (up to an equivalent isotropic medium with intensely fractured rock mass) (use Eq. 3).

Under the conditions where the problem being analysed is intersected by only one or two joint sets, the rock mass is not an equivalent isotropic medium and its strength and behaviour will be dominated by displacements on individual joints. Neither Eqs. 1 nor 3 are valid under these conditions and discontinuum solutions should be used. Therefore, it is important to first define the equivalent isotropic medium.

Schultz (1996) suggested that for an equivalent isotropic medium in a fractured rock mass, the ratio between the scale of the problem and the scale of the rock blocks should be between 5 and 10. Cundall et al. (2008) found, using the quantified method by Cai et al. (2004), that a ratio of up to 20–30 is suitable for this threshold. Priest (1993) stated that the scale of the problem must greatly exceed the block size or fracture spacing. Since neither Priest (1993) nor Hoek and Brown (1980) quantify the ratio, we propose that the ratio of 5–10 suggested by Schultz (1996) is sufficiently large to meet the qualitative description of an equivalent continuous medium as long as the joint set orientations also define roughly isotropic blocks.

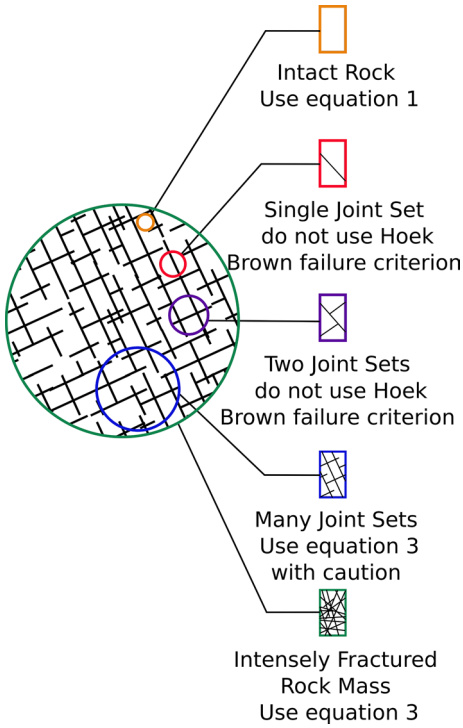

Fig. 4 Schematic of conditions under which the Hoek–Brown failure criterion is valid (Modified from Hoek et al. (1995))

Thus, we suggest that for a ~30 cm diameter wellbore, as is the case for GPK-3 and GPK-4 (see Fig. 1 for location) between 1500 and 4500 m depth (Valley and Evans 2010), the rock mass can be considered intact at the wellbore scale if the fracture density is <5 fractures/m (spacing of 20 cm) and as having many joint sets (thus being isotropic) when the fracture density is greater than 10 fractures/m (spacing of minimum 10 cm). This is represented schematically in Fig. 5 using randomly oriented and located fractures to help visualise how different ranges of fracture frequency would relate to the rock structure descriptions in Fig. 3. A blocky to very blocky rock mass corresponds roughly to Schultz's (1996) suggested ratio of 5–10. For reservoir-scale problems, Fig. 4 should be used to assess which failure criterion should be used to represent the rock mass.

To obtain GSI we used the borehole log data from Genter et al. (1997) and core log data from Genter and Traineau (1996) for EPS-1. We used the fracture count data for 1 m-intervals from Genter et al. (1997) to compute fracture densities. We then used the graphic logs of altered fractured intervals and fracture density from Genter and Traineau (1996) (shown in Fig. 6), in combination with the fracture densities from Genter et al. (1997), to assess the rock structure (using Fig. 3; Marinos et al. 2005). Genter et al. (1997) conducted an assessment of joint set orientation and found two dominant joint sets with dip and dip direction 80/310 and 70/080, while Genter and Traineau (1996) found that the two dominant sets have dip and dip direction of 70/275 and 70/080. Genter et al. (1997) found a minor set with dip and dip direction of 80/270 with two or three random sets, while Genter and Traineau (1996) show stereonets with "a clearly random component of orientation" including approximately 15% of joints with dip of 40° or less, forming a blocky rock mass with intersecting sets. Finally, we used the graphic logs of

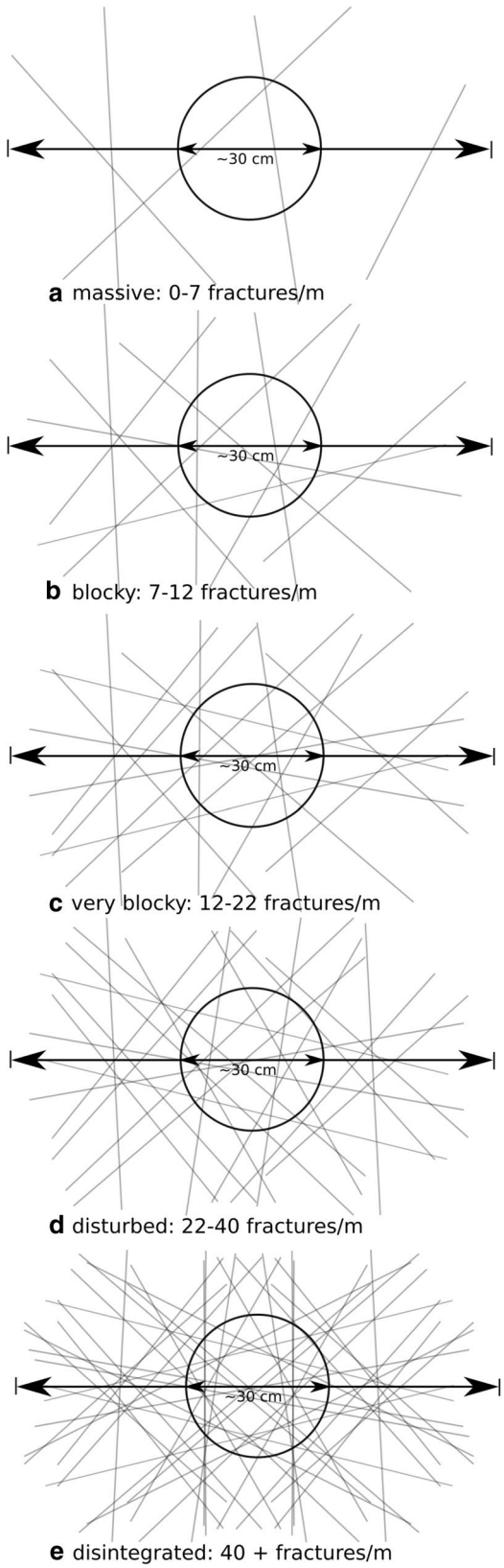

Fig. 5 Example wellbore-rock mass scale conditions for a ~ 30 cm diameter well

cumulative filling width/m and filling types (quartz, hematite, calcite and/or illite) from Genter and Traineau (1996) (Fig. 6) to assess surface condition of the fractures (using Fig. 3; Marinos et al. 2005). Hematite and illite, and the thickness of the infilling, were used to differentiate between good/fair conditions and poor/very poor conditions in Fig. 3; the hematite representing "iron stained surfaces" in the second-to-left category of surface conditions (Fig. 3), and the illite representing "clay coatings or infillings" in the right-most category of the surface conditions (Fig. 3). The thicker the infilling, the farther to the right (decreasing surface quality) the assessment for surface condition was made. We could not assess joint roughness because this was not specified in the logs, however Genter and Traineau (1996) state that "almost all" the fractures are filled with no residual aperture. This suggests that infilling, rather than roughness, will control structure condition, as also found by Cai et al. (2004). Of particular note is that the joints with the widest aperture, and thickest infilling, were associated with intensely fractured zones. For this reason GSI will tend to be particularly low in these areas because of the combination of poor rock mass and joint conditions.

To illustrate our methodology we show, in Fig. 6, three 25 m long intervals with different rock mass characteristics. Interval *A* has an average fracture density of 15 fractures/m, with predominantly thin quartz and hematite filling, and some minor calcite and illite (Fig. 6). The fracture density leads to the assessment of a very blocky structure with some disturbed or blocky intervals. The filling leads to an assessment of a fair to good surface condition (using the GSI chart presented as Fig. 3). The combination of these two assessments results in a range of GSI of 45–55. Intervals *B* and *C* are also shown to provide examples of an excellent and a poor quality rock mass, respectively (Figs. 3 and 6).

We must emphasise that both structure and condition of the rock mass must be assessed for the generalised Hoek–Brown failure criterion. Only characterising the structure does not provide a full representation of the rock mass strength. For example, rocks with similar fracture density (i.e. intervals *A* and *C* with average fracture density of 13–15 fractures/m; Fig. 6) will not have the same GSI if the fracture conditions are different: thin, hematite (iron) staining in interval *A* (assessed as good to fair surface condition) compared to thick illite filling in interval *C* (assessed as very poor to poor surface condition); (Fig. 6). The resulting GSI values are 45–55 and 25–35, respectively (Fig. 3).

With values for m_b, s and a, from Eqs. 4–6 now determined, the final variable required to solve the failure criterion for EPS-1 is the minimum principal stress. We used the minimum horizontal stress (S_{hmin}) calculated for the granite at Soultz-sous-Forêts by Evans (2005) as the minimum principal stress, σ_3', using:

$$s_{hmin} = 0.0130z \tag{7}$$

where z is depth in m.

(See figure on next page.)

Fig. 6 Borehole log data from EPS-1 showing (from left to right): a stratigraphic log showing the altered (black) and relatively unaltered (grey) granite; fracture density (per metre); cumulative filling width (mm per metre); and the infilling type: quartz, hematite, calcite, and illite (shown as "low", "medium", or "high" content). Three 25 m-interval rock masses are labelled A, B, and C (see text and Fig. 3 for details) (Modified from Genter and Traineau (1996))

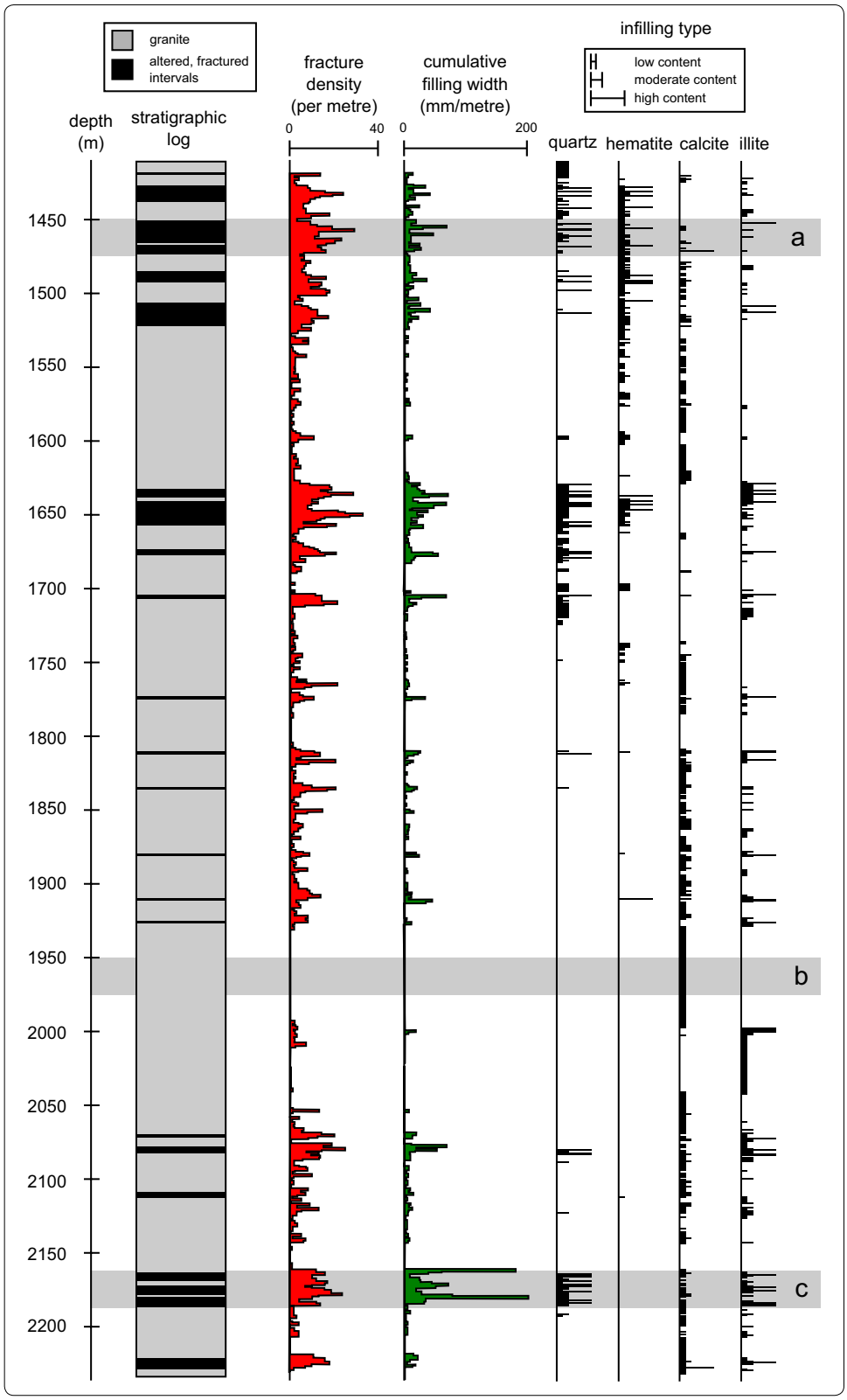
granite
altered, fractured intervals
infilling type
low content
moderate content
high content
depth (m)
stratigraphic log
fracture density (per metre)
0
40
cumulative filling width (mm/metre)
0
200
quartz
hematite
calcite
illite
1450
1500
1550
1600
1650
1700
1750
1800
1850
1900
1950
2000
2050
2100
2150
2200
a
b
c

Table 2 Experimental summary for the compressive deformation experiments performed for this study

Sample number	Depth (m)	Presence of phenocrysts	Bulk dry density (kg/m^3)	Connected porosity	Confining pressure (MPa)	Compressive strength (MPa)	Static elastic modulus (GPa)
1	1420	Not noted	2652	0.0030	0	123.6	N/A
2	1420	Not noted	2650	0.0029	0	N/A	N/A
3	1915	Not noted	2696	0.0018	0	129.2	N/A
4	1915	Not noted	2686	0.0018	0	128.4	N/A
5	1915	Not noted	2682	0.0020	0	146.9	N/A
3A	1558	No	2679	0.0012	0	153.1	53.3
6A	1558	No	2658	0.0012	0	144.6	48.9
2A	1558	No	2672	0.0012	5	263.0	44.1
3C	1558	No	2671	0.0011	10	296.8	57.3
4A	1558	No	2678	0.0011	20	369.5	35.2
5A	1558	No	2666	0.0012	30	433.3	32.9
1A	1558	Yes	2667	0.0012	0	140.6	36.6
2C	1558	Yes	2669	0.0012	0	152.4	47.2
1C	1558	Yes	2656	0.0011	5	255.9	26.0
2B	1558	Yes	2665	0.0009	10	277.2	34.0
3B	1558	Yes	2686	0.0011	20	363.3	35.6
8B	1558	Yes	2639	0.0016	30	380.6	32.0

Experiments were performed at a constant strain rate of 10^{-5} s^{-1}. As noted in the text, the static elastic modulus could not be determined for the samples recovered from depths of 1420 and 1915 m due to technical problems

Rock mass elastic modulus

With estimates for intact elastic modulus (see above), we calculated rock mass elastic moduli, E_{rm}, using the Hoek–Diederichs equation (Hoek and Diederichs 2006):

$$E_{rm} = E_i \left(0.02 + \frac{1 - \frac{D}{2}}{1 + e^{((60+15D-GSI)/11)}} \right) \tag{8}$$

Similarly to the rock mass strength, the E_{rm} is computed along the depth of the borehole using the GSI and the damage factor D. We use $D = 0$ in this study because the rock mass is undamaged and the fractures remain closed; we provide the full Hoek–Diederichs equation for completeness. The Hoek–Diederichs equation follows the same scaling conditions as the Hoek–Brown failure criterion, where E_i (intact elastic modulus) is used for the first scaling condition presented above (intact rock), and E_{rm} from Eq. 8 is used for the second scaling condition (fractured rock mass). A problem falling between these two scaling conditions requires analysis of displacements on discrete structures, as described above.

Results

The connected porosity of the samples ranges between ~0.0012 and ~0.003 (Table 2). Values of uniaxial compressive strength, C_o, vary from ~124 to ~153 MPa (Table 2). There is no systematic difference in porosity or strength between the standard porphyritic granite and the palaeo-weathered porphyritic granite (Table 2). As a result, we do not consider these horizons as mechanically distinct. The average C_o of the tested

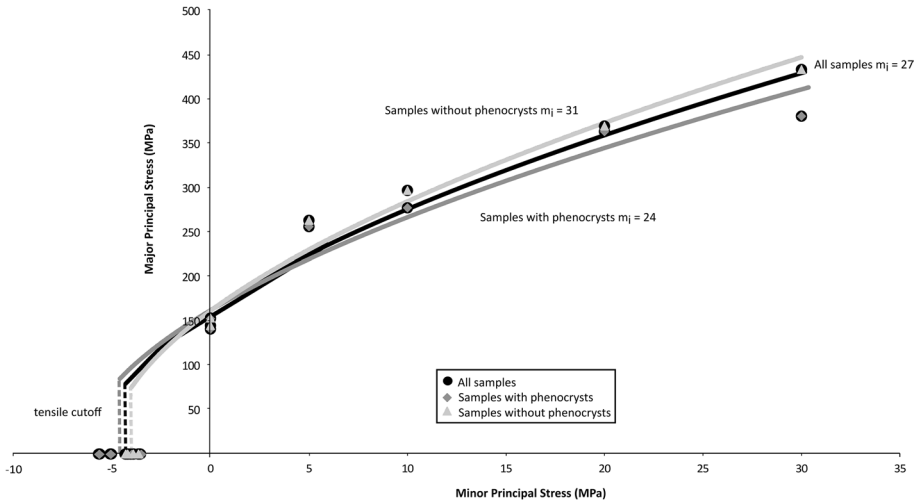

Fig. 7 Triaxial, uniaxial and indirect tensile data and Hoek–Brown failure criterion model fits for the samples from 1558 m depth, showing the fits for samples with and without visible phenocrysts as well as for all samples combined

samples, assumed here to be representative of the standard porphyritic granite from ~1400 to ~2200 m, is ~140 MPa. We also measured no systematic difference between the UCS of the samples from a depth of 1558 m with or without large phenocrysts (Table 2).

Our triaxial experiments show that compressive strength increases as confining pressure is increased (Fig. 7; Table 2). For example, for the samples that contain large phenocrysts, strength is increased from ~145 to ~380 MPa as confining pressure is increased from 0 to 30 MPa (Fig. 7; Table 2). We also measured no systematic difference between the compressive strength of the samples from a depth of 1558 m with or without large phenocrysts over the entire pressure range (Table 2).

Due to the range in measured values for the static modulus in Table 1 (the average of which is ~55 GPa) and our data (in Table 2, the average of which is ~40 GPa), we use a range of elastic modulus values from 30 to 50 GPa to reflect the measured variability while narrowing the range to encompass data obtained through compressive (uniaxial and triaxial) testing. Our data show that, for the samples measured herein, the elastic modulus does not depend on the confining pressure (for the range of confining pressures tested here; Table 2).

The indirect tensile strength results are given in Table 3. The average indirect tensile strengths are 4.0, 4.6 and 4.3 MPa for samples without phenocrysts, with phenocrysts and for all samples, respectively (Table 3).

The Hoek–Brown failure criterion (Eq. 1) model fits for our UCS, triaxial and indirect tensile strength data and their derived m_i values are shown in Fig. 7. The m_i values derived from these granites range from 24 to 31, which is lower than the estimates for granites found in the m_i database in RocData (Rocscience 2017).

The average C_o from our experimental data (140 MPa) is combined with the GSI data estimated from the borehole logs to determine three rock mass failure criteria (Additional file 1), using three values for m_i (25, 30 and 35) chosen to best represent

Table 3 Experimental summary for the indirect tensile deformation experiments performed for this study

Sample number	Presence of phenocrysts	Average thickness (mm)	Average diameter (mm)	Load at tensile rupture (kN)	σ_t (MPa)
4B_2	No	20.14	40.12	5.80	4.17
4B_3	No	24.16	40.12	5.52	3.62
7B_1	No	20.05	40.20	4.90	3.88
7B_2	No	23.81	40.09	6.40	4.27
4B_1	Yes	22.44	40.22	7.12	5.03
4B_4	Yes	21.23	40.18	4.98	3.55
7B_3	Yes	22.13	40.15	7.83	5.61
7B_4	Yes	22.26	40.13	5.65	4.02

σ_t—indirect tensile strength (calculated using Eq. 2)

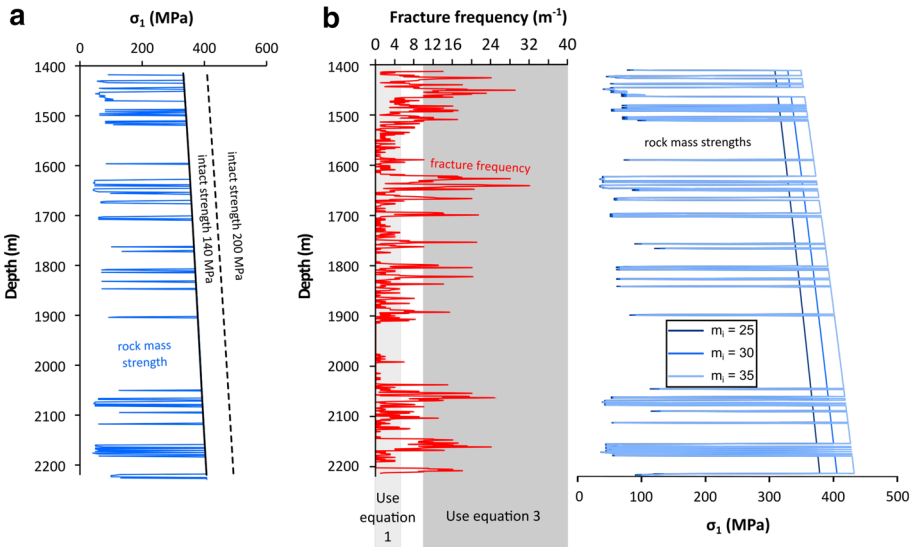

Fig. 8 Hoek Brown failure criteria for EPS-1 over the depth interval 1400–2200 m; **a** comparison of intact strength (using Eq. 1 for $C_o = 140$ MPa (solid line) and 200 MPa (dashed line) and $m_i = 30$, see text for details) and rock mass strength (using Eq. 3) for $C_o = 140$ MPa and $m_i = 30$; **b** comparison of fracture density and resulting rock mass strength for $C_o = 140$ MPa and three different m_i values (25, 30, and 35)

the expected variability based on the experiments shown in Fig. 7 and the suggested value for granite from the m_i database. Figure 8a shows how, for $m_i = 30$, the intact (solid black line) and rock mass strength at the wellbore scale (solid blue line) vary along the length of the borehole, which considers the changing rock mass quality and lithostatic minor principal stress, S_{hmin}, with depth. To determine the stability of the wellbore, using a continuum numerical model for example, the induced minor principal stress, σ_3, would be used explicitly by the modelling software to assess the rock mass strength at any point around the excavation boundary.

For the average C_o, the rock mass strength is lower than the intact rock strength over all intervals with fracture frequency > 10 fractures/m. GSI is 100 for all intervals (Additional file 1) with fracture frequency < 10 fractures/m and therefore

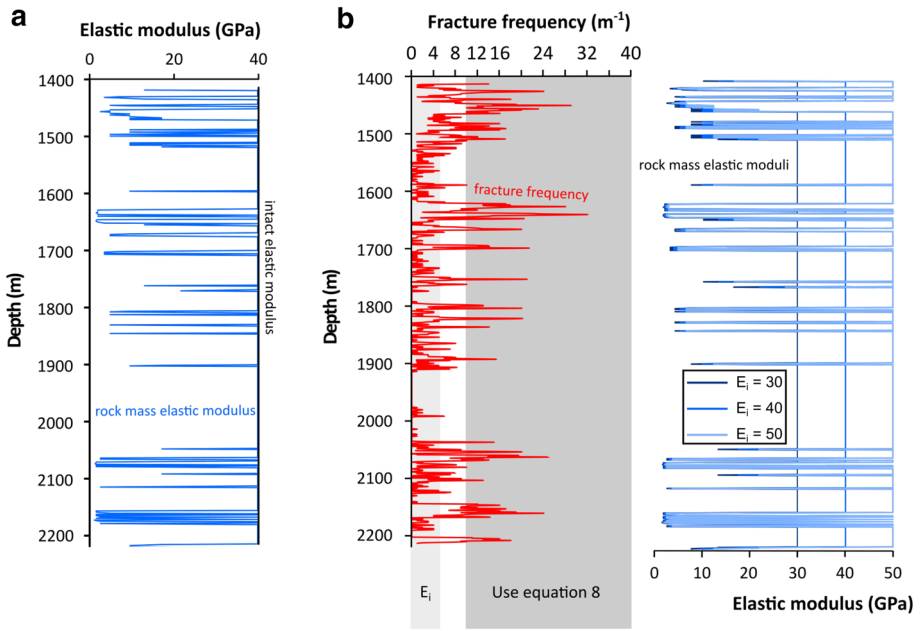

Fig. 9 Elastic modulus for EPS-1 over the depth interval 1400–2200 m; **a** comparison of intact elastic modulus ($E_i = 40$ GPa) and rock mass elastic modulus (using Eq. 8) for $E_i = 40$ GPa; **b** comparison of fracture density and resulting rock mass elastic modulus for three different E_i values (30, 40 and 40 GPa)

the rock mass strength is the same as the intact strength. The fluctuations in rock mass strength for a single C_o are more pronounced than the difference between two intact rock strengths, as shown in Fig. 8a for 140 MPa (solid black line) and 200 MPa (dashed black line).

Figure 8b shows three rock mass failure criteria (for $m_i = 25$, 30 and 35) along with the fracture density (taken from Genter et al. 1997), as a function of depth. The strength is negatively correlated with fracture density (structure), but because GSI is a characterisation of both the structure and the surface conditions, the rock mass strength may be lower than predicted based on fracture density alone, depending on the surface conditions. The joints with the widest aperture and thickest infilling are restricted to the most densely fractured zones, resulting in particularly low GSI in these areas [e.g. at zones A (1450 m) and **c** (2175 m) in Figs. 4 and 8]. Figure 8b shows that the choice of m_i has less impact on rock mass strength when Eq. 3 is used, where the difference in strength between the highest and lowest m_i can be as little as 8 MPa (e.g. 2160 m), than for rock masses where Eq. 1 is used, where the difference can be as much as 50 MPa (e.g. 1937 m).

Similarly, E_i is combined with GSI to determine rock mass elastic modulus, E_{rm}. Figure 9a shows the intact (solid black line) and rock mass (solid blue line) elastic modulus at the wellbore scale for an E_i of 40 GPa. However, unlike rock mass strength (Fig. 8), values of E_{rm} do not take the influence of minor principal stress into account explicitly, but rather through the use of the damage parameter, D (Hoek and Diederichs 2006). The selection of D provides the ability to represent rock masses ranging from damaged with open fractures, as observed in disturbed ground at low minor principle stress ($D = 1$) to undamaged, closed, fully interlocked fractures, as observed

in undisturbed ground at high minor principle stress ($D = 0$). Figure 9a shows that E_{rm} fluctuates considerably with GSI, from 65% of E_i for a GSI of 75–3% of E_i for a GSI of 20.

Figure 9b shows fracture density with depth, plotted alongside three rock mass elastic moduli, determined using three different E_i values ($E_i = 30$, 40 and 50). Similarly to strength (Fig. 8b), E_{rm} is computed using GSI, and is a function of both the structure and the surface conditions. E_{rm} is also less sensitive to the selection of E_i than it is to changes in GSI (Fig. 9b). These low rock mass elastic modulus values are within a similar range as the wireline elastic modulus values for the fractured rock mass shown in Meller and Ledésert (2017).

Discussion

Rock strength and elastic modulus characterisation

Our values of uniaxial compressive strength (Table 2) are consistent with those from the report of Valley and Evans (2006), who found values between 100 and 130 MPa. One of the challenges in determining the strength of this material is that it commonly contains K-feldspar crystals that are very large (long axes up to several tens of mm in length; Fig. 2), however, the rock is dominated by quartz and mica crystals with a long axis of 2–5 mm (Fig. 2). Our sample size—40 mm-diameter cylinders—could be considered too small for laboratory strength testing (the diameter of a sample should be longer than at least ten grains/crystals; Ulusay and Hudson 2007). The twelve experiments of Valley and Evans (2006), which provided similar values to those reported here, were performed on the maximum possible diameter—the diameter of the core (78 mm; samples were 190 mm in length). The average UCS values from this study and from Valley and Evans (2006) were corrected to equivalent 50 mm-diameter strength using the empirical relationship from Hoek and Brown (1980):

$$\sigma_{cd} = \sigma_{50}\left(\frac{50}{d}\right)^{0.18} \tag{9}$$

where σ_{cd} is the strength measured on a sample with diameter, d, and σ_{50} is the equivalent strength of a sample with 50 mm-diameter. The equivalent 50 mm-diameter average C_o values are 137 MPa and 128 MPa for the data from this study and those from Valley and Evans (2006), respectively. Therefore, although the crystal size remains an issue for standard laboratory testing, the values reported in our study are likely representative of, or at least very close to, the uniaxial compressive strength of this material. It is worth noting that we conducted tests on samples with and without visible large phenocrysts, which, when separated, demonstrate that samples without phenocrysts have essentially the same C_o (149 MPa versus 147 MPa), slightly higher m_i (31 versus 24), and slightly lower indirect tensile strength (4.0 MPa versus 4.6 MPa) than samples with phenocrysts. The presence of large phenocrysts in these 40 mm-diameter samples has only a minor effect and average values from all samples can be used for constructing the Hoek–Brown failure criterion.

The average uniaxial compressive strength used in the failure criterion development of this study was determined using experiments performed at room temperature. Although

our estimates of rock mass strength consider the influence of lithostatic (confining) pressure on rock strength (Eq. 3), based on our choice of C_o (i.e. the average of experiments performed at room temperature), we do not consider changes to strength as a result of temperature. The temperature of the granite reservoir was measured to be ~140 °C at the top (~1500 m) and to be ~150 °C at a depth of ~3500 m (Vidal et al. 2015). It is known from experiments and modelling that high temperature (from 100 up to 1000 °C) can influence the short- and long-term strength of granite in the brittle regime (e.g. Wong 1982b; Xu et al. 2008, 2017; Shao et al. 2015; Kumari et al. 2017; Chen et al. 2017; Violay et al. 2017). However, a recent experimental study has shown that the strength of a low-porosity fresh granite is largely unaffected at temperatures of 140–150 °C (Kumari et al. 2017). These new data are in agreement with previously published data that show that temperatures of a couple of hundred degrees Celsius do not appear to greatly influence the short-term strength of granite (Xu et al. 2008; Shao et al. 2015). We further note that our estimates of rock mass elastic modulus do not consider the influence of pressure or temperature. Published data show that static elastic modulus of the same low-porosity, fresh granite increases slightly with increasing pressure and temperature (from ~22 GPa at room temperature up to ~26 GPa at 200 °C; Kumari et al. 2017). Despite these data, it is unclear whether, or to what extent, such temperatures will influence granites from the URG, which are more hydrothermally altered than the granites studied in the aforementioned studies. Future experimental efforts should focus on the influence of temperature on the parameters (strength and elastic modulus) used in the modelling presented herein.

We highlight that the estimates of intact and rock mass strength provided in this study should be considered analogous to the short-term strength of the reservoir rock. Both C_o and m_i are determined from short-term laboratory tests, typically performed at a laboratory strain rate of 10^{-5} s^{-1}. It is well-known that the long-term strength of rock is much lower than its short-term strength, due to the increased influence of time-dependent deformation mechanisms such as stress corrosion cracking (Brantut et al. 2013). Further, in contrast to the short-term strength of granite (Xu et al. 2008; Shao et al. 2015; Kumari et al. 2017), the long-term strength and time-to-failure in granite are considerably reduced by temperatures of a couple of hundred degrees Celsius (Kranz et al. 1982; Xu et al. 2017; Chen et al. 2017). We highlight the long-term strength of granite from the URG (at room temperature and at elevated in situ temperatures) as an interesting avenue for future study.

Failure criterion input parameter considerations

We have shown how the intact and rock mass strength can be computed for any depth using conventional laboratory (C_o and m_i) and borehole characterisation data (to derive GSI) using the Hoek–Brown failure criterion. Triaxial test data are preferred for determining m_i, in particular for intact rock where the m_i can have a large impact on strength at depth. For fractured rock masses, where the generalised Hoek–Brown failure criterion is used, the rock mass strength is much less sensitive to m_i (Fig. 8b) and an estimate from published data (i.e. RocData (Rocscience 2017)) can be sufficient.

We have used the Hoek–Diederichs equation to compute rock mass elastic modulus using conventional laboratory (E_i) and borehole characterisation data. It is preferable

to use E_i values from laboratory testing of the particular intact rock of interest, but for intensely fractured rock masses this value can be estimated because the fractures will tend to dominantly control E_{rm} (Fig. 9b). Published data on the rock of interest could be used or published data on a similar, analogous rock type. Alternatively, E_i can be estimated using (Hoek and Diederichs 2006):

$$E_i = \mathrm{MR} \cdot C_o \tag{10}$$

where MR is a lithology specific factor, which for granite is 300–550 (Hoek and Diederichs 2006). For our average C_o (140 MPa) this would give a range of $E_i = 42–77$ GPa (i.e. similar to the measured values reported in Tables 1 and 2). This simple analysis shows that the elastic modulus of granite from the URG could be estimated using values of uniaxial compressive strength, or vice versa.

Based on the borehole logging data that are available (Genter et al. 1997; Genter and Traineau 1996) we discretised the fracture density into 1 m long intervals. This provides a good representation of the rock mass at the wellbore scale. This interval size effectively differentiates intensely fractured from intact zones. In our analysis, there are three broad zones that contain fracture densities that satisfy scale criterion 2 for rock masses (Fig. 8). Similarly, there are two broad zones that satisfy scale criterion 1 for intact rock. The selection of interval length will depend on the reason for computing the failure criterion and the available data. At wellbore scale, a finer discretisation would be appropriate for obtaining strength and stiffness values for hydraulic stimulation planning, for example. At reservoir scale, a coarser discretisation, perhaps using 10–25 m-intervals, would be more appropriate for modelling variations in stiffness of different units or subunits, for example.

At the wellbore scale (for the GPK wells this is ~ 30 cm at our depth interval of interest) intact rock strengths and elastic moduli should only be used for intervals with fewer than 5 fractures/m, and rock mass strengths and elastic modulus should be used for intervals with greater than 10 fractures/m. These fracture density thresholds will vary depending on the diameter of the well. Rock masses with fracture densities that fall between these should be analysed using discrete methods, such as fracture/fault slip models (e.g. Evans 2005) or using discontinuum numerical modelling methods commonly used at the tunnel scale (e.g. Vardakos et al. 2007; Fekete and Diederichs 2013). Similarly, a fracture density consisting of only parallel joints, rather than intersecting joint sets, should be analysed using discrete methods because of the anisotropic nature of the rock mass.

The intact rock and rock mass characterisation data we used were obtained from drill core, with the ability to test the strength in the laboratory (our data and the data from Valley and Evans (2006)) and high resolution, good quality quantification of structure and surface condition (Dezayes et al. 1995; Genter and Traineau 1996; Genter et al. 1997). However, drill core from geothermal wells will not always be available. In this case, estimations of intact rock strength will rely on surface analogues, cross-well interpolation and verification with drill chips. Wyering et al. (2015) provide a method to estimate rock strength from thin sections or drill chips for hydrothermally altered rocks in geothermal settings. As we have shown, the rock

mass strength is more reliant on GSI than on C_o and m_i; however selecting a reasonable estimate for these values is important.

Genter et al. (1997) showed, for URG granite, that the number of fractures recorded from borehole televiewer (BHTV) logging data was 17% of the number of fractures observed in the core. They found BHTV fracture densities of 0.64 fractures/m, whereas 25 m-interval average fracture densities from the core mapping range from 0.7 fractures/m in massive granite to 9 fractures/m in intensely fractured zones. Evans (2005) similarly show lower fracture densities from BHTV logs than those observed in core in GPK-1. This is partly due to the fact that the televiewer resolution (1–2 mm) is sometimes below the fracture aperture. Fracture statistics from BHTV logging is also dependent on borehole circularity and the quality of the borehole walls, which can depend on rock type, rock mass strength, and alteration amongst others (McNamara et al. 2015). More massive rocks (i.e. those with fewer fractures) tend to have more regular walls and circular diameters, resulting in better quality images (McNamara et al. 2015). We highlight that potential discrepancies between fracture densities derived from BHTV logging data and those measured directly from core must be considered when deriving GSI. While BHTV cannot differentiate small aperture fractures, Genter et al. (1997) show agreement between BHTV and core for locating intensely fractured zones. For the granites from Soultz-sous-Forêts they suggest that fracture densities should be multiplied by two for massive granite and by 13 for intensely fractured zones.

Using rock mass strength and elastic modulus

The ability to quantify the effect of macrofracturing on strength and elastic modulus provides an additional resource for interpreting and predicting well stability and reservoir behaviour. For example, Bérard and Cornet (2003) investigated compressive failure around wells GPK-1 and -2 at Soultz-sous-Forêts using estimates for intact rock strength at a confining pressure of 40 MPa (Rummel and Schreiber 1993). They proposed that time-dependent failure at stresses below the peak strength (i.e. C_o) was responsible for the greater number of compressive failures observed in GPK-1 than in GPK-2, which are both assumed to be in similar lithologies and at similar stress states. Bérard and Cornet (2003) assumed a C_o of 200 MPa, loaded at an effective σ_1 of 144–156 MPa and an effective σ_3 of 0 MPa. Our experiments suggest that the C_o for Soultz-sous-Forêts granite is closer to 140 MPa (see also data from the unpublished report of Valley and Evans (2006)), which would fail immediately if loaded to the effective σ_1 proposed by Bérard and Cornet (2003). In the case of fractured intervals, the equivalent unconfined compressive strength for the rock mass would be even lower, and the rock mass would certainly deform under these conditions. The analysis of Bérard and Cornet (2003) is just one example of the potential use of our values of intact and rock mass strength, which may provide, in this instance, new insight into the discrepancy between the number of compressive failures observed in GPK-1 and GPK-2. In general, assessing the rock mass strength and stiffness of fractured intervals could help with mud weight selection to prevent excessive borehole breakout, washout or wellbore collapse (as defined in Zoback 2010 p. 303–305). They can also enhance the borehole breakout method detailed in

Zoback (2010; p. 231) for determining S_{Hmax} where breakouts have occurred in fractured intervals.

The failure criterion and elastic modulus can be used to inform the locations for hydraulically stimulating a geothermal system. Cipolla et al. (2008) show that pre-existing fractures have a significant impact on the success of hydraulic fracture creation, and that complex fracture networks can be exploited for stimulation. They state that unpropped fracture conductivity is dependent on elastic modulus and closure stress and that fracture complexity cannot be exploited in rocks with elastic modulus less than ~ 13 GPa because of deformation of asperities and proppant embedment. In petroleum systems the elastic modulus that Cipolla et al. (2008) refer to is for intact rock because of the generally soft nature of sedimentary units. In the case of the URG granites the intact rock has high elastic modulus, and rock mass elastic modulus may be more appropriate for stimulation design.

Failure criteria are arguably most important for the numerical modelling of fracturing, permeability and induced seismicity scenarios in reservoirs. For modelling the rock mass as a continuum (as for the matrix in modelling of Deisman et al. 2013; Yoon et al. 2014; Siratovich et al. 2016; Insana et al. 2016) the scale of the model should be considered according to the two scale criteria we employed in this research. The numerical modelling in Siratovich et al. (2016) was conducted at well scale using an intact rock failure criterion, and would only be applicable for rock masses meeting the first scale criterion. The numerical modelling by Yoon et al. (2014) was conducted at reservoir scale using a discontinuum method that incorporates both fracture-specific and rock continuum (in their case intact rock) failure criteria. The discontinuum method is appropriate for discrete faults or fractures, but for distributed intensely fractured zones, such as those observed in the URG, an equivalent continuum for the rock mass may be more appropriate.

Thus far the generalised Hoek–Brown failure criterion has not been empirically established at the reservoir or at the wellbore scales. What we present here should be used as an estimate of lower-bound rock mass strength and stiffness, and to illustrate the impact of fractures on rock mass strength and stiffness. Most importantly we want to emphasise that using intact rock strength without consideration of the weakening and softening effect of fractures can be imprudently under-conservative. We argue that, at the reservoir scale, the effect of using only intact rock failure criteria versus using rock mass failure criteria in fractured zones to model the behaviour of the reservoir must be explored further. This is also true at the small wellbore scale. In addition, the use of the damage parameter, D, to represent damage and interlocking for rock mass stiffness has been empirically developed at excavation boundaries where the minimum principal stress is low. The correct use of this parameter for fully confined reservoir conditions should also be investigated.

Concluding remarks

We present herein a method to estimate the intact and rock mass strength and the rock mass elastic modulus of reservoir rock using easy-to-determine rock properties (uniaxial compressive strength and elastic modulus) and simple-to-use observational methods

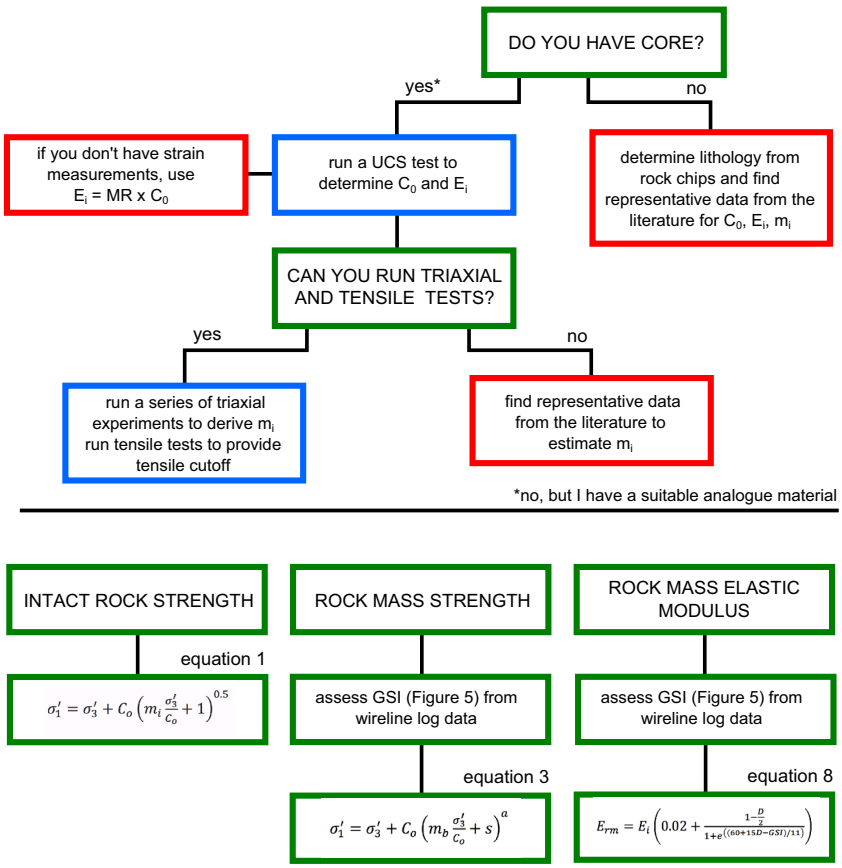

Fig. 10 Flow chart for determining in situ strength (intact and rock mass strength) and rock mass elastic modulus depending on available data. Blue boxes show the recommended route

and formulae (the Hoek–Brown failure criterion and the Hoek–Diederichs equation) (Fig. 10).

We use this method to characterise the URG granite encountered in EPS-1 at Soultz-sous-Forêts and show that there are many intervals where using intact rock strength and stiffness parameters is appropriate given the low fracture density (for example, for a typical wellbore, < 5 fractures/m). In these intervals our laboratory strengths can be used along with previous strength and stiffness data for reservoir and wellbore stability analysis. Numerical models of geothermal reservoirs or wellbores that use strength and stiffness should consider the lower values for these parameters in intensely fractured zones. A better understanding of the impact of fractures on rock mass strength and stiffness will lead to better defined model results for assessing reservoir deformation during exploitation and stimulation, and for determining appropriate drilling programmes for reservoir development, for example mud weight selection during drilling.

We also show that there are many densely fractured intervals where, in our scenario, fracture density exceeds 10 fractures/m and rock mass strength and stiffness parameters should be used. Finally we also show that infilling type is a key aspect of rock mass characterisation, for which hematite and clay infilling information from core or wireline data is crucial. These areas are especially important to characterise because their GSI values

will be particularly low. More focus on identifying fractures and infilling using wireline techniques would allow better rock mass characterisation in the absence of core. In the URG granite there are intervals dominated either by hematite or illite, which modify the rock mass strength differently. Roughness is lacking from these logs, and while we have focussed on infilling, roughness would provide more confidence in the joint condition assessment for joints that lack infilling.

Although triaxial experiments help refine m_i for rock mass strength predictions, we note that using published data from experiments performed on similar rock can be used effectively to provide an estimate. We further note that, in the absence of available core for uniaxial and triaxial compressive strength testing (to find values for strength, elastic modulus and the empirical term m_i), a lithological description of rock chips and a thorough search for published laboratory data will likely provide decent first-order estimates. Especially in intensely fractured intervals, the rock mass strength will be dominated by the rock mass characteristics, such that a first-order estimate of intact strength and stiffness will be sufficient as a starting point. Therefore, armed with a detailed description of the borehole or well wall from wireline log data (fracture density, in particular), one can assess rock mass strength and elastic modulus, important for a wide range of modelling scenarios (e.g. McClure and Horne 2013 and references therein) and stimulation strategies (Cipolla et al. 2008). We recommend that this simple, yet well-established, engineering method be used to characterise geothermal reservoirs worldwide to empirically establish its validity under reservoir and small diameter wellbore conditions. A possible technique would be to measure reservoir deformation during stimulation using distributed deformation measurements in wellbores using fibre optic technology as has been used for rock slope deformation monitoring (e.g. Moore et al. 2010). We also recommend that core and wellbore characterisation be undertaken such that fracture frequency, orientation, infilling and roughness for natural fractures are collected at a resolution that allows computation of the rock mass strength and stiffness criteria. Finally we recommend that wireline techniques, such as gamma ray (Bigelow 1992), be used to explore the possibility of identifying clay infilling signatures for joint condition assessment (as in Meller and Ledésert 2017).

Additional file

Additional file 1. Raw rock mass characterisation assessment used to derive GSI on a 1-m scale.

Authors' contributions
MCV and MJH designed and led the project, and co-wrote the manuscript. MJH, ARLK and PB collected the samples. MCV performed the geotechnical analyses. ARLK measured the connected porosities of the samples taken from depths of 1420 and 1915 m. TQ performed uniaxial compressive strength tests on the samples taken from depths of 1420 and 1915 m. MCV measured the connected porosities of the samples taken from a depth of 1558 m. MCV conducted the uniaxial and triaxial compressive, and indirect tensile strength tests on the samples taken from a depth of 1558 m. All authors contributed to the interpretation of the data and the preparation of the manuscript. All authors read and approved the final manuscript.

Author details
[1] Department of Geological Sciences, University of Canterbury, Private Bag 4800, Christchurch 8140, New Zealand. [2] Géophysique Expérimentale, Institut de Physique de Globe de Strasbourg, (UMR 7516, CNRS, Université de Strasbourg/EOST), 5 rue René Descartes, 67084 Strasbourg cedex, France. [3] Heilongjiang Ground Pressure & Gas Control in Deep Mining

Key Lab, Heilongjiang University of Science and Technology, Harbin 150022, People's Republic of China. [4] Center for Rock Instability and Seismicity Research, Northeastern University, Shenyang 110819, People's Republic of China.

Acknowledgements
We thank Albert Genter, Chrystel Dezayes, Bertrand Renaudié, Chongfeng Chen, Erik Eberhardt, and Mark Diederichs. We also acknowledge the Bureau de Recherches Géologiques et Minières (BRGM) for permission to use existing digital data from fracture network collected on cores and GEIE Exploitation Minière de la Chaleur for providing Soultz core samples. Finally we acknowledge four anonymous reviewers for their detailed comments that helped us communicate our work effectively.

Competing interests
The authors declare that they have no competing interests.

Availability of data and materials
Additional data are available with this manuscript. Additional data can be made available on request to the lead author.

Consent for publication
Not applicable.

Ethics approval and consent to participate
Not applicable.

Funding
MJH and PB acknowledge LABEX grant ANR-11-LABX-0050_G-EAU-THERMIE-PROFONDE; this research therefore benefited from state funding managed by the Agence National de la Recherche (ANR) as part of the "Investissements d'avenir" programme. MJH, ARLK, and PB acknowledge ANR Grant CANTARE (ANR-15-CE06-0014-01). MJH acknowledges a Visiting Erskine Fellowship from the University of Canterbury (New Zealand). TX acknowledges funding from the Natural Science Foundation of China (Grant Nos. 51474051 and 41672301), the National Basic Research Programme (973) of China (Grant No. 2014CB047100), and the Fundamental Research Funds for the Central Universities of China (N150102002). MJH and TX acknowledge a Partenariats Hubert Curien (PHC) Cai Yuanpei grant (Grant Number 36605ZB), jointly managed by the Ministry of Foreign Affairs (MAEDI) and the Ministry of Higher Education and Research (MENESR) in France and the China Scholarship Council (CSC) in China.

Publisher's Note

Received: 23 October 2017 Accepted: 12 June 2018
Published online: 21 June 2018

References

Aichholzer C, Duringer P, Orciani S, Genter A. New stratigraphic interpretation of the Soultz-sous-Forêts 30-year-old geothermal wells calibrated on the recent one from Rittershoffen (Upper Rhine Graben, France). Geotherm Energy. 2016;4:13.
Alber M, Fritschen R, Bischoff M, Meier T. Rock mechanical investigations of seismic events in a deep longwall coal mine. Int J Rock Mech Rock Eng. 2009;46:408–20.
Baria R, Baumgärtner J, Gérard A, Jung R, Garnish J. European HDR research programme at Soultz-sous-Forêts (France) 1987–1996. Geothermics. 1999;28(4):655–69.
Bartier D, Ledésert B, Clauer N, Meunier A, Liewig N, Morvan G, Addad A. Hydrothermal alteration of the Soultz-sous-Forêts granite (Hot Fractured Rock geothermal exchanger) into a tosudite and illite assemblage. Eur J Mineral. 2008;20(1):131–42.
Bérard T, Cornet FH. Evidence of thermally induced borehole elongation: a case study at Soultz, France. Int J Rock Mech Min Sci. 2003;40:1121–40.
Bertuzzi R, Douglas K, Mostyn G. Comparison of quantified and chart GSI for four rock masses. Eng Geol. 2016;202:24–35.
Bieniawski ZT. Engineering rock mass classification. New York: Wiley Interscience; 1989.
Bigelow EL. Introduction to wireline log analysis. Houston: Western Atlas International; 1992.
Blake OO, Faulkner DR, Rietbrock A. The effect of varying damage history in crystalline rocks on the P-and S-wave velocity under hydrostatic confining pressure. Pure Appl Geophys. 2013;170(4):493–505.
Blake OO, Faulkner DR. The effect of fracture density and stress state on the static and dynamic bulk moduli of Westerly granite. J Geophys Res Solid Earth. 2016;121(4):2382–99.
Brace WF, Paulding BW, Scholz CH. Dilatancy in the fracture of crystalline rocks. J Geophys Res Solid Earth. 1966;71(16):3939–53.
Brantut N, Heap MJ, Meredith PG, Baud P. Time-dependent cracking and brittle creep in crustal rocks: a review. J Struct Geol. 2013;52:17–43.
Brideau MA, Pedrazzini A, Stead D, Froese C. Three-dimensional slope stability analysis of South Peak, Crowsnest Pass, Alberta, Canada. Landslides. 2011;8:139–58.
Byerlee JD. Frictional characteristics of granite under high confining pressure. J Geophys Res Solid Earth. 1967;72(14):3639–48.
Cai M, Kaiser P, Uno H, Tasaka Y, Minami M. Estimation of rock mass deformation modulus and strength of jointed hard rock masses using the GSI system. Int J Rock Mech Min Sci. 2004;41(1):3–19.

Chen L, Wang CP, Liu JF, Li Y, Liu J, Wang J. Effects of temperature and stress on the time-dependent behaviour of Beishan granite. Int J Rock Mech Min Sci. 2017;93:316–23.
Cipolla CL, Warpinski NR, Mayerhofer MJ, Lolon EP, Vincent MC. The relationship between fracture complexity, reservoir properties, and fracture treatment design. SPE Annu Tech Conf Exhib. 2008;4:2215–39.
Cundall PA, Pierce ME, Ivars MD. Quantifying the size effect of rock mass strength. In: Potvin Y, Carter J, Dyskin A, Jeffery R, editors. Keynote in proceedings of the 1st first southern hemisphere international rock mechanics symposium, vol. 2, Perth, Australia; 2008 Sept 16–19. p. 15.
Deere DU. Technical description of rock cores for engineering purposes. Felsmechanik und Ingenieurgeologie (Rock Mech Eng Geol). 1963;1(1):16–22.
Deisman N, Khajeh M, Chalaturnyk R. Using geological strength index (GSI) to model uncertainty in rock mass properties of coal for CBM/ECBM reservoir geomechanics. Int J Coal Geol. 2013;112:76–86.
Dezayes C, Villemin T, Genter A, Traineau H, Angelier J. Analysis of fractures in boreholes of hot dry rock project at Soultz-sous-Forêts (Rhine Graben, France). J Sci Drill. 1995;5(1):31–41.
Dezayes C, Villemin T, Pêcher A. Microfracture pattern compared to core-scale fractures in the borehole of Soultz-sous-Forêts granite, Rhine graben, France. J Struct Geol. 2000;22(6):723–33.
Dezayes C, Genter A, Valley B. Structure of the low permeable naturally fractured geothermal reservoir at Soultz. C R Geosci. 2010;342(7):517–30.
Dotta G, Gigli G, Ferrigno F, Gabbani G, Nocentini M, Lombardi L, Agostini A. Geomechanical characterization and stability analysis of the bedrock underlying the Costa Concordia cruise ship. Rock Mech Rock Eng. 2017;50(9):2397–412.
Eberhardt E, Stimpson B, Stead D. Effects of grain size on the initiation and propagation thresholds of stress-induced brittle fractures. Rock Mech Rock Eng. 1999;32(2):81–99.
Eberhardt E. The Hoek-Brown failure criterion. In: Ulusay R, editor. The ISRM suggested methods for rock characterization, testing and monitoring: 2007–2014. New York: Springer; 2012. p. 233–40.
Evans K. Permeability creation and damage due to massive fluid injections into granite at 3.5 km at Soultz: 2. Critical stress and fracture strength. J Geophys Res Solid Earth. 2005. https://doi.org/10.1029/2004JB003168.
Fekete S, Diederichs M. Integration of three-dimensional laser scanning with discontinuum modelling for stability analysis of tunnels in blocky rockmasses. Int J Rock Mech Min Sci. 2013;57:11–23.
Frolova J, Ladygin V, Rychagov S, Zukhubaya D. Effects of hydrothermal alterations on physical and properties of rocks in the Kuril–Kamchatka island arc. Eng Geol. 2014;183:80–95.
Genis M, Basarir H, Ozarslan A, Bilir E, Balaban E. Engineering geological appraisal of the rock masses and preliminary support design, Dorukhan Tunnel, Zonguldak, Turkey. Eng Geol. 2007;92:14–26.
Genter A, Traineau H. Borehole EPS-1, Alsace, France: preliminary geological results from granite core analyses for Hot Dry Rock research. Sci Drill. 1992;3(5):205–14.
Genter A, Traineau H. Analysis of macroscopic fractures in granite in the HDR geothermal well EPS-1, Soultz-sous-Forêts, France. J Volcanol Geotherm Res. 1996;72(1–2):121–41.
Genter A, Castaing C, Dezayes C. Comparative analysis of direct (core) and indirect (borehole imaging tools) collection of fracture data in the Hot Dry Rock Soultz reservoir (France). J Geophys Res Solid Earth. 1997;102(B7):15419–31.
Gérard A, Genter A, Kohl T. The deep EGS (enhanced geothermal system) project at Soultz-sous-Forêts (Alsace, France). Geothermics. 2006;35:473–83.
Géraud Y, Rosener M, Surma F, Place J, Le Garzic É, Diraison M. Physical properties of fault zones within a granite body: example of the Soultz-sous-Forêts geothermal site. C R Geosci. 2010;342(7):566–74.
Griffiths L, Heap MJ, Wang F, Daval D, Gilg HA, Baud P, Schmittbuhl J, Genter A. Geothermal implications for fracture-filling hydrothermal precipitation. Geothermics. 2016;64:235–45.
Guillou-Frottier L, Carré C, Bourgine B, Bouchot V, Genter A. Structure of hydrothermal convection in the Upper Rhine Graben as inferred from corrected temperature data and basin-scale numerical models. J Volcanol Geotherm Res. 2013;256:29–49.
Heap MJ, Faulkner DR. Quantifying the evolution of static elastic properties as crystalline rock approaches failure. Int J Rock Mech Min Sci. 2008;45(4):564–73.
Heap MJ, Kennedy B, Pernin N, Jacquemard L, Baud P, Farquharson J, Scheu B. Mechanical behaviour and failure modes in the Whakaari (White Island volcano) hydrothermal system, New Zealand. J Volcanol Geotherm Res. 2015;295:26.
Heap MJ, Kushnir ARL, Gilg HA, Wadsworth FB, Reuschlé T, Baud P. Microstructural and petrophysical properties of the Permo-Triassic sandstones (Buntsandstein) from the Soultz-sous-Forêts geothermal site (France). Geotherm Energy. 2017;5(1):26.
Hoek E, Brown ET. Empirical strength criterion for rock masses. J Geotech Geoenviron Eng. 1980;106(GT9):1013–35.
Hoek E, Carranza-Torres CT, Corkum B. Hoek-Brown failure criterion. In: Hammah R, Bawden W, Curran J, Telesnicki M, editors. Proceedings of the fifth North American rock mechanics symposium (NARMS-TAC). Toronto: University of Toronto Press; 2002. p. 267–73.
Hoek E, Diederichs MS. Empirical estimation of rock mass modulus. Int J Rock Mech Min Sci. 2006;43(2):203–15.
Hoek E, Kaiser PK, Bawden WF. Support of underground excavations in hard rock. Rotterdam: Balkema; 1995. ISBN 9789054101871.
Hoek E, Carter TG, Diederichs MS. Quantification of the geological strength index chart. 47th US rock mechanics/geomechanics symposium San Francisco, CA, USA June 23–26; 2013.
Hooijkaas GR, Genter A, Dezayes C. Deep-seated geology of the granite intrusions at the Soultz EGS site based on data from 5 km-deep boreholes. Geothermics. 2006;35(5):484–506.
Insana A, Barla M, Elmo D. Multi scale numerical modelling related to hydrofracking for deep geothermal energy exploitation. Procedia Eng. 2016;158:314–9.
Kappelmeyer O, Gérard A, Schloemer W, Ferrandes R, Rummel F, Benderitter Y. European HDR project at Soultz-sous-Forêts: general presentation. Geotherm Sci Technol. 1991;2(4):263–89.
Kumari WGP, Ranjith PG, Perera MSA, Shao S, Chen BK, Lashin A, Arifi NA, Rathnaweera TD. Mechanical behaviour of Australian Strathbogie granite under in situ stress and temperature conditions: an application to geothermal energy extraction. Geothermics. 2017;65:44–59.

Kushnir ARL, Heap MJ, Baud P. Assessing the role of fractures on the permeability of the Permo-Triassic sandstones at the Soultz-sous-Forêts (France) geothermal site. Geothermics. 2018;74:181–9.
Kranz RL, Harris WJ, Carter NL. Static fatigue of granite at 200 °C. Geophys Res Lett. 1982;9(1):1–4.
Ledésert B, Dubois J, Genter A, Meunier A. Fractal analysis of fractures applied to Soultz-sous-Forêts hot dry rock geothermal program. J Volcanol Geotherm Res. 1993;57(1–2):1–17.
Ledésert B, Berger G, Meunier A, Genter A, Bouchet A. Diagenetic-type reactions related to hydrothermal alteration in the Soultz-sous-Forêts granite, France. Eur J Min. 1999;11(4):731–41.
Ledésert B, Hebert R, Genter A, Bartier D, Clauer N, Grall C. Fractures, hydrothermal alterations and permeability in the Soultz enhanced geothermal system. C R Geosci. 2010;342(7):607–15.
Li D, Wong L. The Brazilian disc test for rock mechanics applications: review and new insights. Rock Mech Rock Eng. 2013;46:269–87.
Lockner DA. A generalized law for brittle deformation of Westerly granite. J Geophys Res Solid Earth. 1998;103(B3):5107–23.
Magnenet V, Fond C, Genter A, Schmittbuhl J. Two-dimensional THM modelling of the large scale natural hydrothermal circulation at Soultz-sous-Forêts. Geotherm Energy. 2014;2(1):17.
Marinos V, Marinos P, Hoek E. The geological strength index: applications and limitations. Bull Eng Geol Environ. 2005;64:55–65.
Martin C, Kaiser P, McCreath D. Hoek–Brown parameters for predicting the depth of failure around tunnels. Can Geotech J. 1999;36:136–51.
McClure M, Horne RN. Discrete fracture network modeling of hydraulic stimulation: coupling flow and geomechanics. New york: Springer Science & Business Media; 2013. https://doi.org/10.1007/978-3-319-00383-2.
McNamara D, Massiot C, Lewis B, Wallis I. Heterogeneity of structure and stress in the Rotokawa geothermal field, New Zealand. J Geophys Res Solid Earth. 2015;120:1243–62.
Meller C, Ledésert B. Is there a link between mineralogy, petrophysics, and the hydraulic and seismic behaviours of the Soultz-sous-Forêts granite during stimulation? A review and reinterpretation of petro-hydromechanical data toward a better understanding of induced seismicity and fluid flow. J Geophys Res Solid Earth. 2017;122:9755–74. https://doi.org/10.1002/2017JB014648.
Moore JR, Gischig V, Button E, Loew S. Rockslide deformation monitoring with fiber optic strain sensors. Nat Hazards Earth Syst Sci. 2010;10:191–201.
Muramoto FS, Elders WA. Correlation of wireline log characteristics with hydrothermal alteration and other reservoir properties of the Salton Sea and Westmorland geothermal fields, Imperial Valley, California. Los Alamos: Los Alamos National Laboratory, USA; 1984.
Oda M, Katsube T, Takemura T. Microcrack evolution and brittle failure of Inada granite in triaxial compression tests at 140 MPa. J Geophys Res Solid Earth. 2002;107:2233. https://doi.org/10.1029/2001JB000272.
Pola A, Crosta G, Fusi N, Barberini V, Norini G. Influence of alteration on physical properties of volcanic rocks. Tectono. 2012;566–567:67–86.
Pola A, Crosta G, Fusi N, Castellanza R. General characterization of the mechanical behaviour of different volcanic rocks with respect to alteration. Eng Geol. 2014;169:1–13.
Pells PJ, Bieniawski ZT, Hencher SR, Pells SE. Rock quality designation (RQD): time to rest in peace. Can Geotech J. 2017;54(6):825–34.
Pribnow D, Schellschmidt R. Thermal tracking of upper crustal fluid flow in the Rhine Graben. Geophys Res Lett. 2000;27(13):1957–60.
Priest SD. Discontinuify analysis for rock engineering. London: Chapman & Hall; 1993.
Richards L, Read S. New Zealand greywacke characteristics and influence on rock mass behaviour. The second half century of rock mechanics. In: 11th congress of the international society for rock mechanics, Lisbon. London: Taylor & Francis; 2007.
Rocscience Inc. 2017. https://www.rocscience.com.
Rummel F. Physical properties of the rock in the granitic section of borehole GPK1, Soultz-sous-Forêts. Geothermal Energy in Europe: the Soultz Hot Dry Rock Project; 1992. p. 199–216.
Rummel F, König E. Physical properties of core samples, borehole EPS1, Soultz-sous-Forêts: velocity, density- and magnetic susceptibility-logs, depth interval 933–2227 m, Yellow report 6, Ruhr-Universität, Bochum, unpublished report; 1991. p. 58.
Rummel F, Schreiber D. Physical properties of the core K21, borehole GPK1, Soultz-sous-Forêts, depth interval 3522.58–3525.88 m, Yellow report 12, Ruhr-Universtität, Bochum, unpublished report; 1993. p. 11.
Rummel F, te Kamp L, Schäfer T. Fracture mechanic properties of granite cores from GPK1, Yellow report 7, Ruhr-Universität, Bochum, unpublished report; 1989. p. 20.
Rummel F, König E, Thieme B. Fracture mechanics parameters of EPS1 Soultz granite cores, Yellow Report 10, Ruhr-Universität, Bochum, unpublished report; 1992. p. 44.
Sano O, Kudo Y, Mizuta Y. Experimental determination of elastic constants of Oshima granite, Barre granite, and Chelmsford granite. J Geophys Res Solid Earth. 1992;97(B3):3367–79.
Sari M. An improved method of fitting experimental data to the Hoek–Brown failure criterion. Eng Geol. 2012;127:27–35.
Sausse J, Fourar M, Genter A. Permeability and alteration within the Soultz granite inferred from geophysical and flow log analysis. Geothermics. 2006;35(5):544–60.
Sausse J, Dezayes C, Dorbath L, Genter A, Place J. 3D model of fracture zones at Soultz-sous-Forêts based on geological data, image logs, induced microseismicity and vertical seismic profiles. C R Geosci. 2010;342(7):531–45.
Schaefer L, Oommen T, Corazzato C, Tibaldi A, Escobar-Wolf R, Rose W. An integrated field-numerical approach to assess slope stability hazards at volcanoes: the example of Pacaya, Guatemala. Bull Volcanol. 2013;75(6):720–38.

Schäfer T. Ultraschallunguntersuchungen an Granitbohrkerne der Bohrung Soultz-sous-Forêts bezüglich einer Abschätzung von in situ Spannungen anhand von Riessschliessungdrücken, Diploma thesis. Bochum: Ruhr-Universität; 1990. p. 119.
Schultz RA. Relative scale and the strength and deformability of rock masses. J Struct Geol. 1996;18(9):1139–49.
Shen J, Priest SD, Karakus M. Determination of Mohr-Coulomb shear strength parameters from generalized Hoek-Brown criterion for slope stability analysis. Rock Mech Rock Eng. 2012;45:123–9.
Shao S, Ranjith PG, Wasantha PLP, Chen BK. Experimental and numerical studies on the mechanical behaviour of Australian Strathbogie granite at high temperatures: an application to geothermal energy. Geothermics. 2015;54:96–108.
Siratovich PA, Heap MJ, Villeneuve MC, Cole JW, Kennedy BM, Davidson J, Reuschlé T. Mechanical behaviour of the Rotokawa Andesites (New Zealand): insight into permeability evolution and stress-induced behaviour in an actively utilised geothermal reservoir. Geothermics. 2016;64:163–79.
Surma F, Geraud Y. Porosity and thermal conductivity of the Soultz-sous-Forêts granite. In: Thermo-hydro-mechanical coupling in fractured rock. Basel: Birkhäuser; 2003; p. 1125–36.
Tapponnier P, Brace WF. Development of stress-induced microcracks in Westerly granite. Int J Rock Mech Min Sci Geomech Abstr. 1976;13(4):103–12.
Traineau H, Genter A, Cautru JP, Fabriol H, Chevremont P. Petrography of the granite massif from drill cutting analysis and well log interpretation in the geothermal HDR borehole GPK1 (Soultz, Alsace, France). Geotherm Sci Technol. 1991;3(1–4):1–29.
Tullis J, Yund RA. Experimental deformation of dry Westerly granite. J Geophys Res. 1977;82(36):5705–18.
Ulusay R, Hudson J. The complete ISRM suggested methods for rock characterization, testing and monitoring: 1974–2006. Antalya: Elsevier; 2007.
Valley B, Evans KF. Strength and elastic properties of the Soultz granite. In: EHDRA scientific conference, Soultz-sous-Forêts, France; 2006. p. 15–6.
Valley B, Evans KF. Stress heterogeneity in the granite of the Soultz EGS reservoir inferred from analysis of wellbore failure. In: Proceedings of world geothermal congress 2010; 2010.
Vardakos SS, Gutierrez MS, Barton NR. Back-analysis of Shimizu Tunnel No. 3 by distinct element modeling. Tunn Undergr Space Technol. 2007;22:401–13.
Vidal J, Genter A, Schmittbuhl J. How do permeable fractures in the Triassic sediments of Northern Alsace characterize the top of hydrothermal convective cells? Evidence from Soultz geothermal boreholes (France). Geotherm Energy. 2015;3(1):8.
Vidal J, Genter A, Chopin F. Permeable fracture zones in the hard rocks of the geothermal reservoir at Rittershoffen, France. J Geophys Res Solid Earth. 2017. https://doi.org/10.1002/2017jb014331.
Violay M, Heap MJ, Acosta M, Madonna C. Porosity evolution at the brittle-ductile transition in the continental crust: Implications for deep hydro-geothermal circulation. Nat Sci Rep. 2017;7(1):7705.
Wong TF. Micromechanics of faulting in Westerly granite. Int J Rock Mech Min Sci Geomech Abstr. 1982a;19(2):49–64.
Wong TF. Effects of temperature and pressure on failure and post-failure behaviour of Westerly granite. Mech Mater. 1982b;1(1):3–17.
Wyering LD, Villeneuve MC, Wallis IC, Siratovich PA, Kennedy BM, Gravley DM, Cant JL. Mechanical and physical properties of hydrothermally altered rocks, Taupo Volcanic Zone, New Zealand. J Volcanol Geotherm Res. 2014;288:76–93.
Wyering LD, Villeneuve MC, Wallis IC, Siratovich PA, Kennedy BM, Gravley DM. The development and application of the alteration strength index equation. Eng Geol. 2015;199:48–61.
Yoon JS, Zang A, Stephansson O. Numerical investigation on optimized stimulation of intact and naturally fractured deep geothermal reservoirs using hydro-mechanical coupled discrete particles joints model. Geothermics. 2014;52:165–84.
Xu XL, Feng GAO, Shen XM, Xie HP. Mechanical characteristics and microcosmic mechanisms of granite under temperature loads. J China Univ Min Technol. 2008;18(3):413–7.
Xu T, Zhou GL, Heap MJ, Zhu WC, Chen CF, Baud P. The influence of temperature on time-dependent deformation and failure in granite: a mesoscale modeling approach. Rock Mech Rock Eng. 2017. https://doi.org/10.1007/s00603-017-1228-9.
Zhang C, Chu W, Liu N, Zhu Y, Hou J. Laboratory tests and numerical simulations of brittle marble and squeezing schist at Jinping II hydropower station, China. J Rock Mech Geotech Eng. 2011;3(1):30–8.
Zoback MD. Reservoir geomechanics. Cambridge: University Press; 2010. ISBN 978-0-521-146197.